International Journal of GEOMATE, April, 2026 Vol.30, Issue 140, pp.76-85
ISSN: 2186-2982 (P), 2186-2990 (O), Japan, DOI: https://doi.org/10.21660/2026.140.g15208
Geotechnique, Construction Materials and Environment

EXTRACTION OF SLOPE VARIATION EXTENT USING OPTICAL SENSORS AND SAR FOR THE MANASLU CIRCUIT TRAIL, NEPAL

*Hijiri Shimojima[1]

[1]Faculty of Regional Environment Science, Tokyo University of Agriculture, Japan

*Corresponding Author, Received: 22 July 2025, Revised: 12 Jan. 2026, Accepted: 15 Jan. 2026

ABSTRACT: Frequent slope deformation areas induced by intense monsoonal rainfall in Nepal threaten trekking routes and local infrastructure, especially in high-altitude regions like the Manaslu Circuit Trail. This study evaluates the effectiveness of satellite-based landslide detection methods using both optical and synthetic aperture radar (SAR) data. Two optical-based techniques (land cover change classification and Normalized Difference Vegetation Index (NDVI)- Gray Size Index (GSI) differencing) and five SAR-based approaches (texture analysis, Normalized Difference Polarization Index (NDPI) differencing, dual-polarization image interpretation, coherence difference analysis, and interferogram interpretation) were applied to pre- and post-monsoon Sentinel-1 and Sentinel-2 datasets. A field survey conducted in September 2024 provided ground-truth data for validating remote sensing results. Among all methods, optical approaches produced more reliable detection results, with NDVI–GSI differencing demonstrating the highest accuracy. SAR-based techniques faced challenges due to terrain-induced distortions and coherence loss, though coherence difference analysis showed relative promise. Limitations in optical imagery, such as misclassification caused by seasonal land use changes, suggest that SAR data can complement optical analysis to improve reliability. This study concludes that a hybrid approach integrating optical and SAR datasets enhances landslide detection in mountainous regions.

Keywords: Landslide, SAR, Optical Sensor, Trail, Manaslu Conservation Area, Nepal

1. INTRODUCTION

Nepal, a mountainous country in South Asia, attracts tourists from around the world for Himalayan mountaineering and trekking in its foothills [1][2]. These activities provide a vital source of foreign income and significantly contribute to local economic development [3]. The Himalayan region represents one of the country's most important tourism assets [4].

However, Nepal experiences frequent natural hazards such as floods, landslides, and debris flows triggered by heavy rainfall during the monsoon season [5]. Landslides often interrupt key transportation routes, disrupting logistics networks and causing considerable economic losses that have become a major societal issue.

Such slope disasters frequently occur in the Higher Himalaya region, located north of the Main Central Thrust (MCT). Trekking trails traversing this area are also susceptible to landslides. Due to narrow and rugged terrain and the absence of well-developed roads, these trails serve as the sole means of transportation not only for trekkers but also for local residents. When a landslide occurs along a trail, it hinders mobility for both community members and goods transportation.

Identifying the locations of past landslides is essential for predicting future landslide occurrences and contributes to disaster mitigation measures such as early countermeasures and evacuation planning [6]. Research on landslide occurrence locations can generally be classified into three categories, depending on the focus and methodological approach: (1) studies evaluating the structural characteristics of areas prone to landslides based on subsurface geological conditions; (2) spatial analytical methods using GIS to identify zones with high susceptibility; and (3) studies involving hazard modeling and catchment-scale analyses of landslide occurrence.

Previous studies addressing the structural characteristics of landslide-prone areas include investigations estimating subsurface structures in landslide regions of Indonesia [7] and studies focusing on precursor detection and monitoring techniques for slope failures [8]. In terms of GIS-based spatial analyses, prior research has examined the spatial distribution of landslide susceptibility in newly constructed road areas in northern Bali, Indonesia [9]. Furthermore, hazard modeling and catchment-scale analyses have been conducted in Nepal and other regions to develop landslide occurrence probability maps and watershed-scale hazard maps [10].

Compared with landslides occurring in suburban or rural areas, landslides along trekking trails are generally smaller in scale and involve limited traffic and transport volumes, as these routes are primarily used for the movement of people, livestock, and small quantities of goods. As a result, such landslides have received relatively limited attention and remain understudied. Nevertheless, even small-scale landslides along trekking trails can cause serious disruptions to supply transport and the mobility of

both local residents and trekkers. Despite advances in landslide research, most existing studies focus on suburban or rural hilly areas, whereas mountainous regions intensively used for trekking have been rarely examined.

Accurately identifying the location and extent of slope deformation along trails is essential for sustainable trail maintenance and management. Various satellite-based approaches have been shown to be effective in detecting landslides adjacent to road networks. Previous studies have applied optical sensor imagery, such as Landsat, to identify landslide sites [11] and used ensemble learning models on aerial photographs [12]. However, these optical systems are weather-dependent and often face challenges acquiring high-quality data during unfavorable conditions.

To address this issue, Synthetic Aperture Radar (SAR) data, which can observe Earth's surface regardless of atmospheric conditions or time of day, has emerged as a promising tool for disaster monitoring. Especially since the 2015 major earthquake in central Nepal, numerous studies—such as that of Bekaert et al. [13]—have investigated slope failure detection using SAR imagery. Nevertheless, research specifically focusing on landslides occurring along trekking trails remains limited. Thus, identifying landslide occurrence locations along trekking routes using satellite imagery and other remote sensing data can contribute not only to infrastructure safety management for local communities but also to ensuring the stable and sustainable use of these areas by trekkers.

This study aims to evaluate the effectiveness of existing landslide extraction methods for accurately delineating slope deformation areas using optical and SAR data, specifically along trekking routes in Nepal.

The remainder of this paper is structured as follows. Section 2 discusses the significance of the study. Section 3 describes the study area and the methods used to extract landslide locations along the trekking trail using Sentinel-1/2 optical and SAR data. Section 4 presents and discusses the analytical results, and Section 5 provides the conclusions and implications of the findings.

2. RESEARCH SIGNIFICANCE

This study evaluates the effectiveness of existing landslide extraction methods using optical and SAR data along trekking routes in Nepal, with the aim of accurately identifying slope deformation areas. For the optical sensor data, two approaches were applied: RGB-NDVI Color Composite for the Land Cover Distribution Chart (LCDC) and NDVI-GSI Differential Analysis. For the SAR data, five methods were employed: texture analysis, NDPI differential analysis, dual-polarization SAR image interpretation, coherence difference analysis, and interferogram interpretation. A comparison of these methods indicates that landslide detection along mountainous trekking routes can be improved by primarily utilizing optical sensor data while supplementing it with SAR imagery. This combined approach enables clearer differentiation between actual landslides and land-use changes, resulting in more detailed and accurate extraction. Such improvements contribute not only to infrastructure safety management for local communities but also to enhanced risk management and more stable tourism use by trekkers.

3. METHODOLOGY

3.1 Study Area

The target area for this study is the Manaslu Circuit Trail located in the Gorkha region, approximately 200 km northwest of Kathmandu, the capital of Nepal. This circular trekking route encircles Mount Manaslu, which stands at an elevation of 8,156 meters. The high-altitude section of the trail is designated as the Manaslu Conservation Area (Fig. 1).

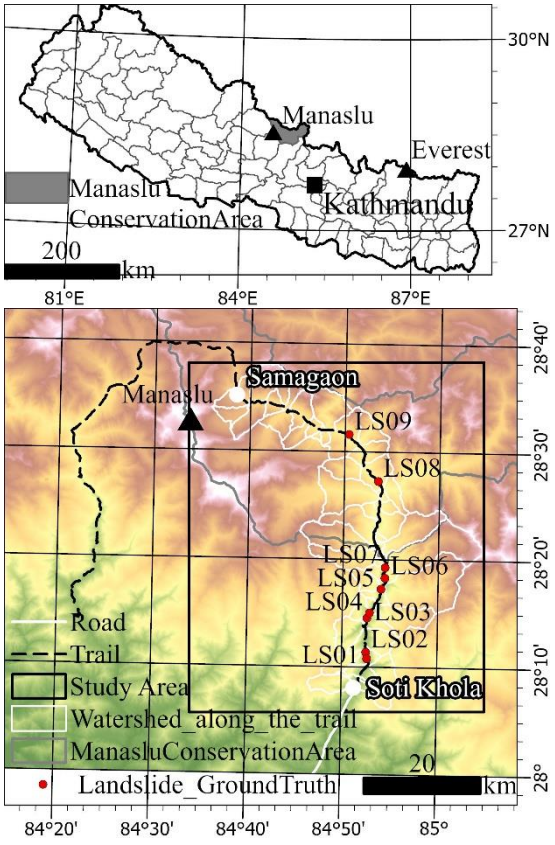

Fig.1 Study area map

3.2 Date Sources

To extract landslide-affected areas along the Manaslu Circuit Trail, optical and SAR sensor data were utilized. Specifically, Sentinel-2 optical

imagery and Sentinel-1 SAR imagery were selected. To capture slope deformation dynamics, one pre-monsoon and one post-monsoon scene were selected for each sensor. For Sentinel-2 imagery, cloud-free scenes within the study area were preferentially selected. The specifications of the datasets used in the analysis are summarized in Table 1.

Table 1 Data Sources

Type	Satellite name	Acquisition date	Orbit	Polarization
Optical Satellite Imagery	Sentinel -2	2024.4.29	—	—
		2024.10.21	—	—
SAR Imagery	Sentinel -1	2024.5.03	Ascending	VV, VH
		2024.5.27		VV, VH
		2024.10.06		VV, VH
		2024.4.17	Descending	VV, VH
		2024.5.11		VV, VH
		2024.9.20		VV, VH

3.3 Landslide Extraction Methods

In this study, following previous research [14][15], multiple approaches were employed to extract landslides. For optical sensor data, two methods were applied: land cover change classification maps and Normalized Difference Vegetation Index (NDVI)–Gray Size Index (GSI) differential analysis. For SAR data, five methods were implemented: texture analysis, Normalized Difference Polarization Index (NDPI) differential analysis, interpretation of dual-polarization SAR images, coherence differential analysis, and interferogram interpretation. To identify landslides occurring along the trail, two spatial scopes were defined: (1) catchment areas adjacent to the trail, and (2) buffer zones of 50 meters from the trail route.

3.3.1 RGB-NDVI Color Composite for the Land Cover Distribution Chart (LCDC)

This method identifies landslide areas by detecting changes in vegetation between two periods. NDVI values before and after the monsoon were calculated from Sentinel-2 data. A color composite image was created by assigning pre-monsoon NDVI to red, post-monsoon NDVI to green, and pre-monsoon blue band reflectance to blue [16][17]. The resulting image was classified into five colors (red, yellow, green, blue, black), with red regions interpreted as landslide-affected areas. A supervised classification using the Maximum Likelihood Method was then applied using training areas extracted from these color classes.

3.3.2 NDVI-GSI Differential Analysis

This method identifies landslide areas as regions that transitioned from vegetated surfaces NDVI before the monsoon to bare surfaces GSI afterward [18]. GSI was calculated using Equation (1):

$$GSI = \frac{(R - B)}{(R + G + B)} \quad (1)$$

Where *R*, *G*, and *B* represent the reflectance of red, green, and blue bands from Sentinel-2 imagery. Thresholds for NDVI and GSI were determined through visual inspection of false-color satellite images (The NDVI thresholds were set to 0.2 (pre-monsoon) and 0.3 (post-monsoon). The GSI threshold pre- monsoon is 0.1, and post-monsoon is 0.06).

3.3.3 SAR Intensity Texture Analysis

Texture analysis using SAR intensity data was conducted to delineate sediment disaster zones, which typically exhibit rough surface textures due to disrupted land cover [19][20]. Pre-monsoon VV-polarized SAR images were converted to backscatter coefficients (σ^0) and filtered with a 5×5 Lee filter to suppress speckle noise. Landslide-prone areas were identified based on the standard deviation of σ^0, as such regions show significantly elevated SD values.

Thresholds were statistically defined using the mean and standard deviation of the SD values, with five levels set: $\mu + 1.0\sigma$ to $\mu + 3.0\sigma$. Given the radar illumination geometry, ascending scenes captured west-facing slopes and descending scenes east-facing slopes. To ensure comprehensive extraction, both datasets were merged, and the same procedure was applied throughout the analysis.

3.3.4 Normalized Difference Polarization Index (NDPI) Differential Analysis

NDPI was applied to detect changes in surface scattering characteristics using pre- and post-monsoon VV and VH polarization backscatter data [21]. NDPI is defined as (Equation2):

$$NDPI = \frac{(\sigma^0 VV - \sigma^0 VH)}{(\sigma^0 VV + \sigma^0 VH)} \quad (2)$$

In this study, σ0VV and σ0VH represent the backscatter coefficients (σ0) of VV and VH polarizations, respectively. The NDPI, ranging from −1.0 to 1.0, was used to distinguish volume scattering (e.g., vegetation) from surface scattering (e.g., bare ground). NDPI was calculated from pre- and post-monsoon SAR data, and the absolute difference between the two was derived. Areas affected by sediment-related disasters typically show a shift from volume to surface scattering, resulting in high absolute NDPI difference values. However, contributions from snow and ice scattering complicate threshold selection. Therefore, five statistical thresholds were defined: $\mu + 1.0\sigma$ to $\mu + 3.0\sigma$.

3.3.5 Dual-Polarization SAR Image Interpretation

A color composite image was created using VV and VH polarizations before the monsoon and VV polarization after the monsoon. Bare landslides, which exhibit increased VV reflectance over time, were interpreted as purple regions [22][23].

3.3.6 Coherence Difference Analysis

Coherence Values (CV) are generated during the interferometric SAR processing and represent the correlation coefficient between intensity data acquired at two different times, ranging from 0 to 1.0. Low CV indicate weak temporal correlation in land cover, suggesting that surface conditions have changed between acquisitions [24][25].

In this study, coherence was calculated separately from pre-monsoon and post-monsoon SAR image pairs. The coherence derived from the post-monsoon pair was subtracted from that of the pre-monsoon pair on a pixel-by-pixel basis. Areas affected by sediment-related disasters are typically characterized by a transition to bare ground, resulting in low coherence difference values relative to the overall distribution.

Therefore, five threshold levels were defined based on the statistical distribution of the coherence differences: $\mu - 1.0\sigma$, $\mu - 1.5\sigma$, $\mu - 2.0\sigma$, $\mu - 2.5\sigma$, and $\mu - 3.0\sigma$.

3.3.7 Interferogram Interpretation

An interferogram is an image represented by fringe patterns in a color chart generated through interferometric SAR (InSAR). InSAR is a technique that interferes two SAR datasets acquired at different times to measure elevation and ground deformation from phase differences. The interferogram displays phase differences within a range from $-\pi$ to $+\pi$. A phase difference of π indicates that the round-trip distance of the microwave has changed by one wavelength between the two observation periods. Consequently, areas with gradual surface deformation are represented by widely spaced fringes, whereas areas with abrupt surface deformation are represented by closely spaced fringes. Since landslide-affected areas exhibit elevation changes before and after the event, they were interpreted as disaster sites based on the presence of closely spaced fringes in the interferogram.

3.3.8 Ground-truth Survey

To validate the remote sensing-derived landslide detection results, a field survey was conducted along the Manaslu Circuit Trail between September 8–21, 2024. Landslide sites were verified visually and recorded with photographs and GPS coordinates. Interviews with local residents were also conducted to gather temporal data on disaster occurrences. These records served as ground-truth data for evaluating the accuracy of satellite-based extraction methods.

4. RESULTS AND DISCUSSION

4.1 Landslide Extraction Using RGB-NDVI Color Composite for the LCDC

The results of landslide extraction based on land cover change classification using optical sensor data are shown in Fig. 2. Within the trail buffer zone, a total of 213 landslide sites were extracted, covering an area of 40.7 hectares. Of the nine ground-truth sites, two were correctly extracted. The remaining seven sites were not detected, which suggests that no landslide events occurred at those locations in 2024. Subsequently, 141 random points were generated within the extracted landslide areas. Using post-monsoon Sentinel-2 imagery and satellite images from Google Earth as reference data, the proportion of correctly matched points (accuracy) was calculated (Table3). The accuracy was 78.0%; however, due to a high number of points being classified outside actual landslide areas, both the F-measure and Cohen's kappa coefficient yielded relatively low values. Misclassification primarily occurred in farmland, livestock grazing areas, riverbanks, and residential settlements. These errors are presumed to have resulted from changes in NDVI values between the two observation periods, leading to false positives in the extraction process.

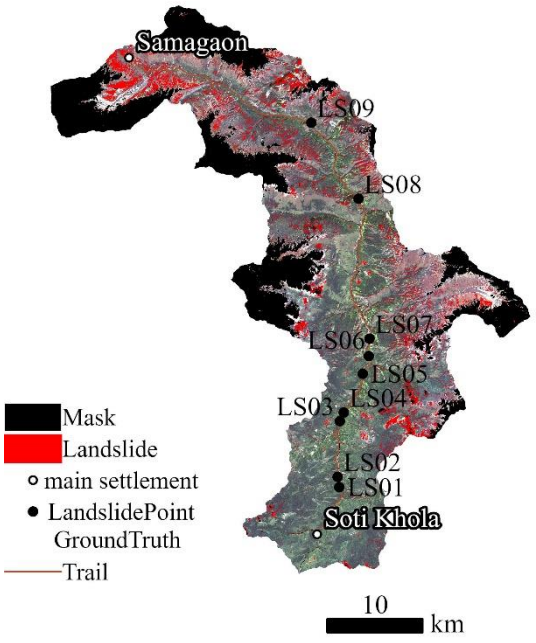

Fig. 2 Landslide Extraction Using RGB-NDVI Color Composite for the LCDC

4.2 Landslide Extraction Using NDVI-GSI Differential Analysis

The NDVI-GSI differential analysis results are

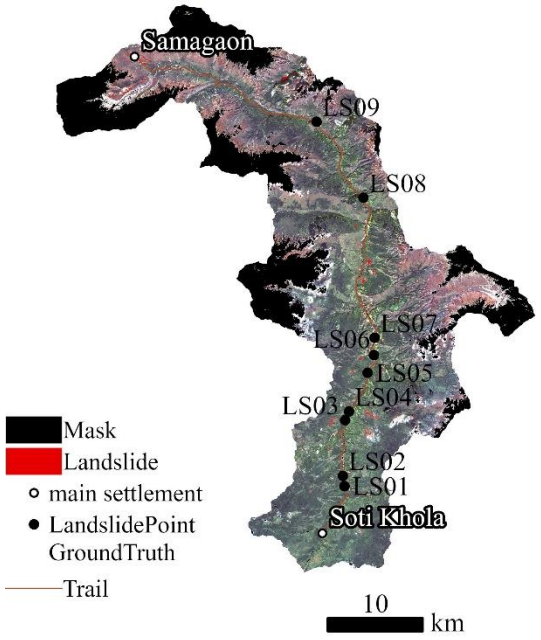

Fig. 3 Landslide Extraction Using NDVI–GSI Differential Analysis

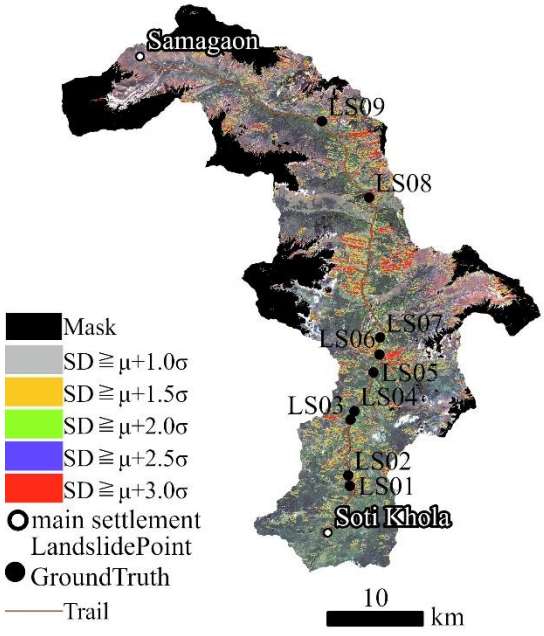

Fig. 4 Landslide Extraction Using SAR Intensity-Based Texture Analysis

presented in Fig. 3. A total of 99 landslide-affected sites were extracted within the trial buffer zone, encompassing an area of 13.0 hectares. Of the nine ground-truth sites, two were correctly identified. The remaining seven sites were not detected, which suggests that no landslide events occurred at those locations in 2024.

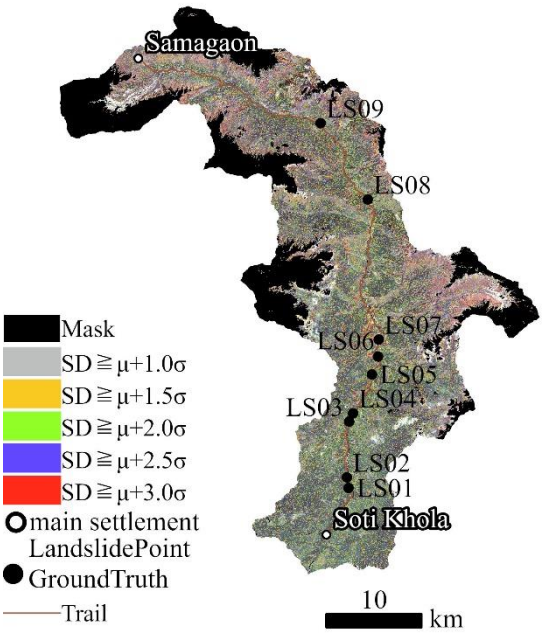

Fig. 5 Landslide Extraction Using NDPI Differential Analysis

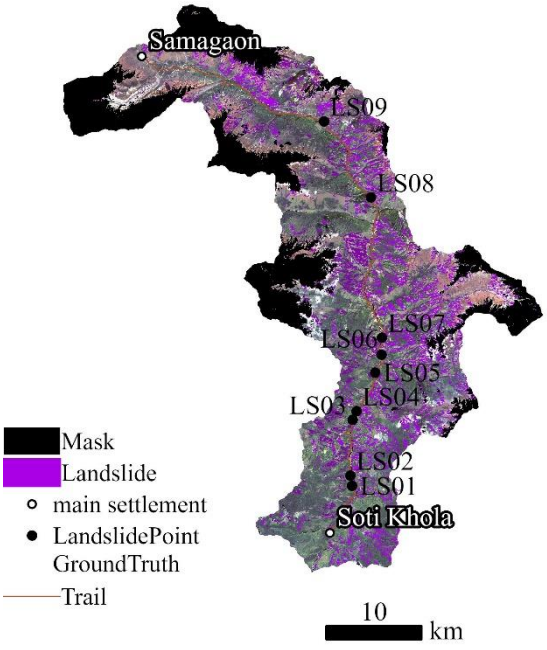

Fig. 6 Landslide Extraction Using Dual-Polarization SAR Composite Imagery

The accuracy was 81.3%, which was higher than that obtained by any other method (Table3). However, due to a large number of points being classified outside actual landslide areas, both the F-measure and Cohen's kappa coefficient yielded relatively low values. Misclassified areas were similar to those observed in the land cover change classification map, including farmland, livestock grazing zones, riverbanks, and residential settlements. Compared to

the land cover change classification map, the total extracted area was smaller. This underestimation is presumed to be a result of the threshold values set for NDVI and GSI, which may have led to conservative extraction of landslide-affected regions.

4.3 Landslide Extraction Using SAR Intensity-Based Texture Analysis

Texture analysis and NDPI differential analysis results, based on SAR backscatter coefficients, are shown in Fig. 4 and Fig. 5, respectively. The texture analysis tended to highlight ridge and valley regions based on thresholding, while NDPI-based results showed extensive and fragmented patterns that were difficult to interpret as landslide zones [26].

These challenges are likely due to geometric distortions in SAR imagery, such as layover and shadowing. In comparison with ground-truth data, texture analysis correctly identified four out of nine sites, while NDPI analysis detected only two. The accuracy was 68.0% for the texture-based analysis method and 60.7% for the NDPI differential analysis (Table 3).

4.4 Landslide Extraction Using Dual-Polarization SAR Image Interpretation

Fig. 6 presents the results derived from dual-polarization SAR imagery. Similar to other SAR-based approaches, the image interpretation was hindered by layover and radar shadow effects, resulting in unreliable detection. Only one of the nine ground-truth sites was correctly identified, indicating the limitations of this method in mountainous terrain. The accuracy was 74.0% (Table 3).

4.5 Landslide Extraction Using Coherence Difference Analysis

Landslide extraction results from coherence difference analysis are shown in Fig. 7. Although spatial patterns were scattered, five of the nine ground-truth sites were successfully matched. The accuracy was 64.0% (Table 3). This suggests that coherence-based methods may offer relatively better results than SAR intensity analyses, although some matches may have occurred coincidentally.

4.6 Landslide Extraction through Interferogram Interpretation

The interferogram shown in Figure 8 displays fringe patterns in certain areas, which are considered indicative of crustal deformation. However, overall coherence was insufficient for reliable fringe interpretation. The interferometric processing was conducted using data pairs acquired in April or May and in September or October. Due to the large temporal baseline between these observations, the coherence of the data was significantly reduced.

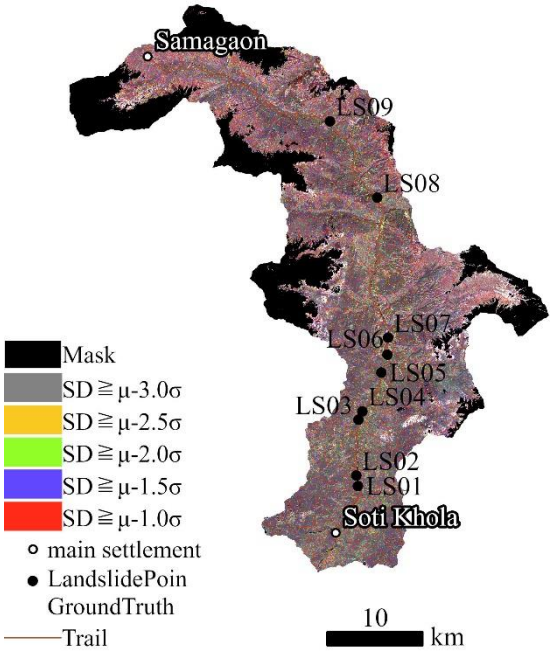

Fig. 7 Landslide Extraction Using Coherence Difference Analysis

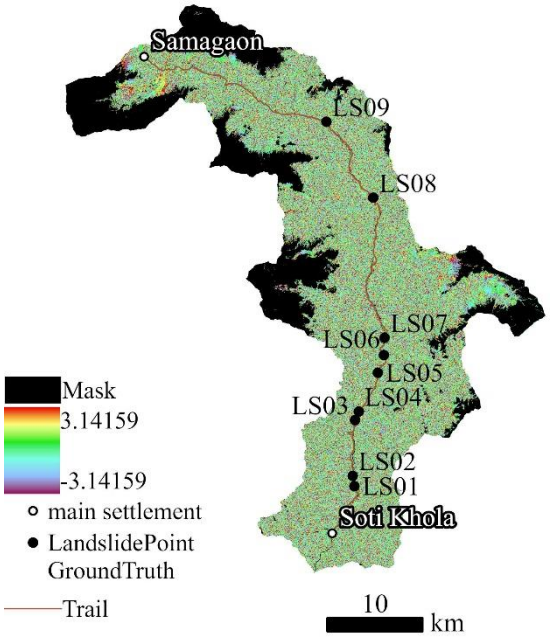

Fig. 8 Landslide Identification from Interferometric SAR Imagery

4.7 Landslide Extraction Results Based on Ground-truth Comparison

Table 2 presents a comparative evaluation of the

Table 2 Comparison Between Ground Truth Locations and Landslide-Affected Areas Extracted by Each Method

No	Photo of Landslide	LCDC	NDVI-GSI	Texture Analysis	NDPI Difference Analysis	DPSII	Coherence Difference Analysis
LS01		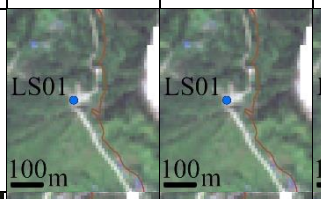		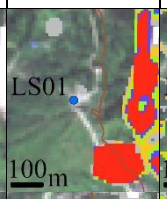	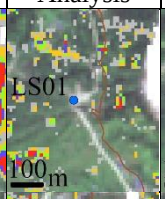	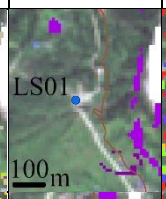	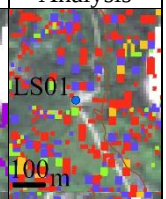
LS02		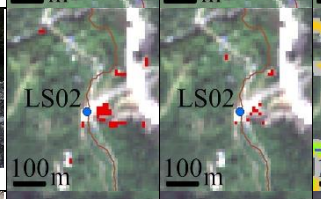		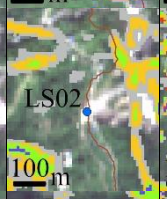	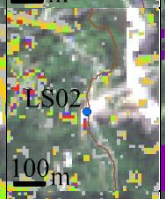	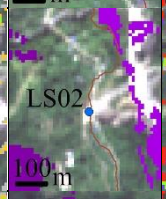	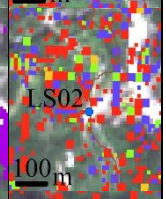
LS03		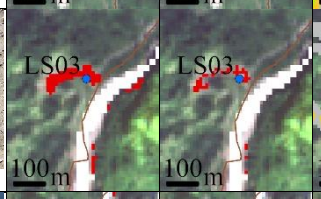		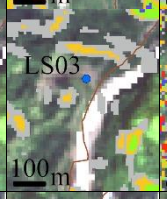	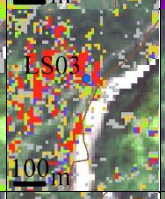	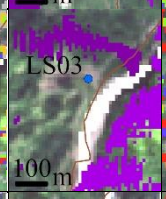	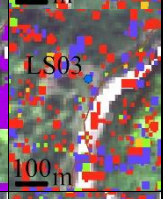
LS04		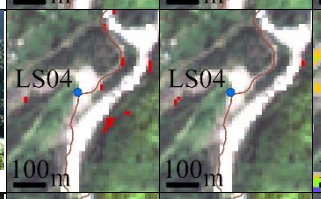		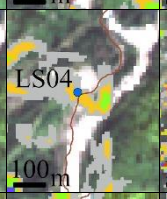	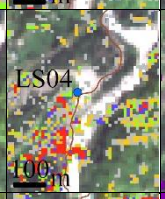	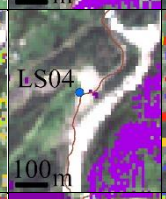	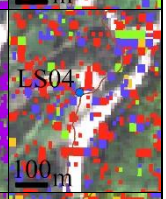
LS05		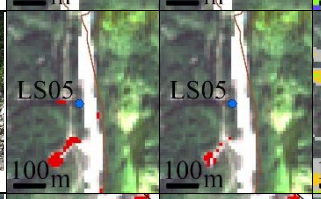		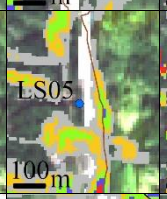	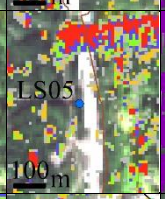	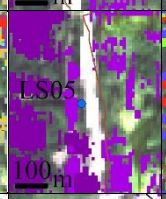	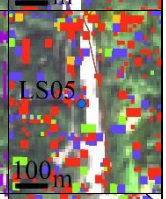
LS06		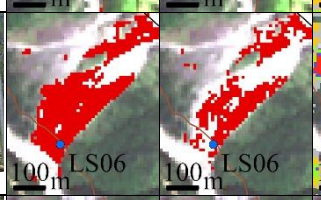		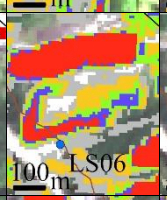	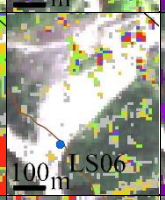		
LS07							
LS08							
LS09							

Table 3 Results of Landslide Detection for Nine Ground-Truth Locations Across Multiple Analytical Methods

		Optical Satellite Imagery						SAR Imagery											
		LCDC			NDVI-GSI			Texture Analysis			NDPI DA			DPSII			Coherence DA		
		L	O	T	L	O	T	L	O	T	L	O	T	L	O	T	L	O	T
Ground Truth	L	2	7	9	2	7	9	4	5	9	2	7	9	1	8	9	5	4	9
	O	0	0	0	0	0	0	0	0	0	0	0	0	0	0	0	0	0	0
Validation data	L	3	25	28	2	26	28	11	17	28	3	25	28	9	19	28	9	19	28
	O	8	114	122	2	120	122	31	91	122	34	88	122	20	102	122	35	87	122
	T	11	139	150	4	146	150	42	108	150	37	113	150	29	121	150	44	106	150
Accurancy(%)		78.0			81.3			68.0			60.7			74.0			64.0		
F-measure		0.154			0.125			0.314			0.092			0.316			0.250		
Kappa Coefficiant		0.054			0.082			0.116			-0.153			0.155			0.028		

Legend: L: Landslide, O: Others, T: Total

results obtained from various analytical methods concerning nine ground-truth locations (LS01–LS09).

At LS01, no landslide area was detected by either optical or SAR datasets, suggesting that no slope deformation occurred at this site in 2024. LS02 yielded a small-scale landslide detection using optical sensor analysis; SAR-based methods indicated partial detection, but layover and radar shadow effects likely reduced data reliability.

LS03 showed consistent detection across both data sources, although slight spatial mismatches were observed. Optical data did not detect LS04, but SAR-based methods identified slope deformation areas to some extent, again with limitations due to terrain-induced distortion. LS05 yielded similar results to LS04.

LS06 was detected by both optical and SAR data and corresponded to the most extensive landslide in the study area, with an estimated width of approximately 100 meters and a length of 400 meters. This was the only site where interviews with nearby residents were conducted, confirming that heavy rainfall in August 2024 triggered the slope deformation areas.

At LS07, no landslide was detected using either data source, indicating the absence of deformation. LS08 revealed a small-scale landslide using optical data and partial detection through SAR, but terrain distortions compromised accuracy. LS09 produced similar results to LS08, and both sites are unlikely to have experienced slope deformation areas in 2024.

These findings suggest that when slope deformation is observed by both optical and SAR datasets, the site can be reliably classified as a landslide area. In contrast, SAR-only detection in mountainous regions should be interpreted cautiously due to layover and radar shadowing effects. Optical-only detections may reflect land use changes, such as seasonal agricultural activity, and cannot be unequivocally identified as landslides. Therefore, a combined approach using both optical and SAR data is essential for accurate landslide extraction in complex mountain environments.

5. CONCLUSION

In this study, we applied two optical-based and four SAR-based methods to extract landslide-affected areas along the Manaslu Circuit Trail in Nepal. Each method was evaluated in terms of its capacity to delineate slope failure zones, and its effectiveness was validated using ground-truth data.

Consistent with previous findings, the complex topography of the Himalayan region poses significant challenges for SAR-based landslide detection due to layover, shadowing, and coherence loss. Among the SAR approaches, coherence difference analysis yielded comparatively better results, although its accuracy remained limited.

On the other hand, the NDVI-GSI differential analysis using optical sensor data demonstrated the most promising performance, effectively identifying landslide sites with fewer false positives. However, its susceptibility to seasonal land cover changes, particularly agricultural activities, highlights limitations in discriminating between genuine landslides and anthropogenic surface changes.

For landslide detection in mountainous regions, optical sensor data remain the most effective primary source while minimizing misclassification through time-series analysis of NDVI fluctuations. Furthermore, by incorporating SAR imagery to differentiate between actual landslides and land use changes, more detailed and accurate extraction of landslide-affected areas can be achieved.

In this study, the SAR dataset was limited to C-band Sentinel-1 imagery. To enhance the potential for landslide detection, a key challenge lies in incorporating SAR data acquired in the L-band,

which, due to its longer wavelength, can penetrate vegetated areas more effectively. This would allow for improved observation of surface deformation and facilitate the identification of optimal image pairs for interferometric SAR (InSAR) analysis.

These findings contribute to improved understanding of remote sensing-based disaster monitoring in high-altitude regions, supporting more effective trail management and community resilience in Nepal's mountainous landscapes.

6. ACKNOWLEDGMENTS

This field survey was made possible through a sponsored research donation from Mr. Yoichi Nakata. I would like to take this opportunity to express my sincere gratitude. I thank Mr. Ram Raj Rijal(Executive Director) and staff from Himalaya Research Expeditions(P) LTD., who have totally supported our fieldwork in Manaslu Base Camp and Manaslu Conservation Area, Nepal. In addition, I am grateful to Mr. Naruo Katte and Mr. Shou Shimojima for their valuable cooperation in conducting the field survey.This work was supported by JSPS KAKENHI Grant Numbers JP22K12623, JP25K03332.

7. REFERENCES

1. Sherpa A. T. and Shrestha H. P., Mountain tourism and Nepal's mountain tourism policy: An overview. PYC Nepal Journal of Management, 4(1) 2011, pp.76‑92. https://doi.org/10.3126/pycnjm.v4i1.81580
2. Nyaupane G. P., Lew A. A., and Tatsugawa K., Perceptions of trekking tourism and social and environmental change in Nepal's Himalayas. Tourism Geographies, 16(3) 2014, pp415‑437. DOI:10.1080/14616688.2014.942233
3. Bhattarai K., Upadhyaya G., and Bohara S. K., Tourism, Employment Generation and Foreign Exchange Earnings in Nepal. Journal of Tourism and Hospitality Education, 11 2021, pp.1‑21. doi:10.3126/jthe.v11i0.38232
4. Wall I., Adventure Tourism in Nepal. Journal of Tourism and Himalayan Adventures, 1(1) 2019, pp.46‑67. https://doi.org/10.3126/jtha.v1i1.81289
5. Benfield A., Impact forecasting Nepal: Earthquake event recap report. Aon Benfield, 2015, pp. 3–32.
6. Pardeshi S. D., Autade S. E. and Pardeshi S. S., Landslide hazard assessment: recent trends and techniques. SpringerPlus, 2 2013, Article 523., pp.1-11. doi:10.1186/2193-1801-2-523
7. Nishimura I., Noguchi T., Ono Y. and Kohno M., Subsurface structures based on microtremor observations in landslide area of Tandikat, West Sumatra, Indonesia. International Journal of GEOMATE, 22(90) 2022, pp. 57–62. https://geomatejournal.com/geomate/article/view/1029
8. Sugimoto S. and Ishizuka Y., Slope deformation monitoring using wireless sensor network and evaluation of mechanical stability by FDM simulation. International Journal of GEOMATE, 22(94) 2022, pp. 13–20. https://geomatejournal.com/geomate/article/view/97
9. Diara I. W., Suyarto R. and Saifulloh M., Spatial distribution of landslide susceptibility in new road construction Mengwitani–Singaraja, Bali, Indonesia based on geospatial data. International Journal of GEOMATE, 23(96) 2022, pp. 95–103. https://geomatejournal.com/geomate/article/view/3320
10. Dahal R. K., Hasegawa S., Bhandary N. P., Poudel, P. P., Nonomura A. and Yatabe R., A replication of landslide hazard mapping at catchment scale. Geomatics, Natural Hazards and Risk, 3(2) 2012, pp. 161–192. doi:10.1080/19475705.2011.629007
11. Le T. T. T. and Kawagoe S., Study on landslide category based on temporal-spatial characteristic distribution in northern Vietnam using satellite images. International Journal of GEOMATE, 14(43) 2018, pp. 118–124. https://geomatejournal.com/geomate/article/view/1592.
12. Opara J. N., Moriwaki R. and Chun P.J., Ensemble learning-based automatic detection of landslide areas from aerial photographs. International Journal of GEOMATE, 27(122) 2024, pp. 79–86. https://geomatejournal.com/geomate/article/view/4761
13. Bekaert D. P. S., Handwerger A. L., Agram P. and Kirschbaum D. B., InSAR-based detection method for mapping and monitoring slow-moving landslides in remote regions with steep and mountainous terrain: An application to Nepal. Remote Sensing of Environment, 249 2020, Article 111983. doi:10.1016/j.rse.2020.111983
14. Phakdimek S., Komori D. and Chaithong T. T., Combination of optical images and SAR images for detecting landslide scars using a classification and regression tree. International Journal of Remote Sensing, 44(11) 2023, pp. 3572–3606. doi:10.1080/01431161.2023.2224096
15. Kouno T., Inoue Y., Ito T. and Kuwahara Y., Extraction of landslide areas in the northern mountainous region of Nepal using SAR and optical sensors. Environmental Information Science, 31 2017, pp. 241–246. [in Japanese with English abstract] doi:10.11492/ceispapers.ceis31.0_241

16. Sader S. A. and Winne J. C., RGB-NDVI colour composites for visualising forest change dynamics. International Journal of Remote Sensing, 13(16) 1992, pp. 3055–3067. doi:10.1080/01431169208904102
17. Pujiono E., Kwak D.A., Lee W.K., Sulistyanto, Kim S.R., Lee J. Y., Lee S.H., Park T. and Kim M.I., RGB-NDVI color composites for monitoring the change in mangrove area at the Maubesi Nature Reserve, Indonesia. Forest Science and Technology, 9(4) 2013, pp. 171–179. doi:10.1080/21580103.2013.842327
18. Xiao J., Shen Y., Tateishi R. and Bayaer W., Development of topsoil grain size index for monitoring desertification in arid land using remote sensing. International Journal of Remote Sensing, 27(12) 2006, pp. 2411–2422. doi:10.1080/01431160600554363
19. Pingxiang L., and Shenghui F., SAR image classification based on its texture features. Geo-Spatial Information Science, 6 2003, pp. 16–19. doi:10.1007/BF02826887
20. Chen S., Useya J. and Mugiyo H., Decision-level fusion of Sentinel-1 SAR and Landsat 8 OLI texture features for crop discrimination and classification: Case of Masvingo, Zimbabwe. Heliyon, 6 Article e05358 2020, pp.1-14 doi:10.1016/j.heliyon.2020.e05358
21. Cao Y.G., Yan, L.J. and Zheng Z.Z., Extraction of information on geology hazard from multi-polarization SAR images. The International Archives of the Photogrammetry, Remote Sensing and Spatial Information Sciences, 37(B4) 2008, pp. 1529–1532.
22. Uhlmann S. and Kiranyaz S., Classification of dual- and single-polarised SAR images by incorporating visual features. ISPRS Journal of Photogrammetry and Remote Sensing, 90 2014, pp. 10–22. doi:10.1016/j.isprsjprs.2014.01.005
23. Zhou T., Li Z. and Pan J., Multi-feature classification of multi-sensor satellite imagery based on dual-polarimetric Sentinel-1A, Landsat-8 OLI, and Hyperion images for urban land-cover classification. Sensors, 18(2) 2018, Article 373. pp.1-20 doi:10.3390/s18020373
24. Jung J. and Yun S.H., Evaluation of coherent and incoherent landslide detection methods based on synthetic aperture radar for rapid response: A case study for the 2018 Hokkaido landslides. Remote Sensing, 12(2) 2020, Article 265. pp.1-26 doi:10.3390/rs12020265
25. Tzouvaras M., Danezis C. and Hadjimitsis D. G., Small-scale landslide detection using Sentinel-1 interferometric SAR coherence. Remote Sensing, 12(10) 2020, Article 1560. pp. 1-33 doi:10.3390/rs12101560
26. Burrows K., Walters R. J., Milledge D. and Densmore A. L., A systematic exploration of satellite radar coherence methods for rapid landslide detection. Natural Hazards and Earth System Sciences, 20 2020, pp. 3197–3214. doi:10.5194/nhess-20-3197-2020